

Design Aspects of a Novel Topology Air-Cored Permanent Magnet Linear Generator for Direct Drive Wave Energy Converters

Rieghard Vermaak, *Member, IEEE*, and Maarten J. Kamper, *Senior Member, IEEE*

Abstract—Direct drive wave energy converters are attractive due to the elimination of intermediate mechanical power conversion stages. Longitudinal flux (LF) linear generators with iron-cored stators have so far been dominant in experimental direct drive WECs, but suffer from high bearing loads and unwanted end effects. A novel linear air-cored topology is presented in this paper which eliminates most of the end effects associated with LF iron-cored machines as well as the attraction forces between iron-cored stators and magnet translators. The attraction forces between the opposing sides of the translators of double-sided air-cored machines are also ideally eliminated. An analytical model and an exhaustive optimization procedure for finding the minimum active mass subject to certain performance specifications are developed for the novel topology. Finite element analysis is used to verify and further analyze the model. First test results from a 1 kW experimental machine correspond well with designed values and confirm the feasibility of implementing the novel topology on a small scale.

Index Terms—Air-cored, analytical models, design optimization, direct drive, electrical machines, finite element methods, linear generator, nonoverlapping windings, permanent magnet (PM), wave energy.

NOMENCLATURE

a	Number of parallel circuits per phase.
A_g	Air gap area (m ²).
A_m	Permanent magnet area (m ²).
B_r	Permanent magnet residual flux density (T).
γ_{cu}	Copper density (kg/m ³).
γ_{fe}	Permanent magnet density (kg/m ³).
δ	Ratio of end winding to active winding length.
d_w	Wire diameter (m).
φ	Magnetic Flux (Wb).
f_{dt}	Total instantaneous force developed (N).
g	Mechanical air gap (m).
h	Stator height (m).
H_c	Permanent magnet coercive field strength (A/m).
h_m	Average magnet height (m).
i	Instantaneous phase current (A).

I	RMS phase current (A).
κ	Per-unit coil coil-side width.
k_f	Copper fill factor.
L	Generator active length (m).
ℓ	Active winding length (m).
ℓ_g	Total air gap length (m).
L_s	Synchronous phase inductance (H).
μ_0	Permeability of free space (H/m).
μ_{rec}	Permanent magnet recoil permeability.
N	Number of turns per coil.
n_c	Number of parallel strands per coil turn.
n_s	Number of stator sections.
p	Number of active poles.
q	Number of coils per phase.
Q	Total number of coils.
θ_c	Coil width (rad).
θ_m	Magnet width (rad).
θ_p	Pole width (rad).
ρ_{cu}	Resistivity of copper (Ω m).
R_s	Phase resistance (Ω).
τ_m	Magnet width to pole pitch ratio.
v	Instantaneous translator velocity (m/s).
ω	Electrical frequency (rad/s).

I. INTRODUCTION

THE ocean is a very attractive renewable energy source, not least because it covers around three quarters of the earth's surface [1] and energy can be extracted from the waves, tides, currents, temperature gradients, and salinity gradients in the ocean [2]. Wave energy, in particular, is spatially more concentrated than both wind and solar energy [3]; it is also more persistent [3] and predictable than wind energy [4]. The global wave power resource has been estimated to be at least 1 TW, with a potential annual energy production of about 2000 TWh [1], [4]; this is comparable to the energy production from nuclear or hydropower in 2006.

Many different wave energy converters (WECs) have been proposed to harness this enormous energy resource, although no superior technology is yet apparent [2], [5]. WECs need to be robust enough to handle the harsh conditions of the sea; they must also be maintenance free as far as possible, because maintenance at sea can be expensive, difficult, and dangerous. Due to the variability of the waves, high part-load efficiency is also desirable for WECs [6].

Manuscript received December 21, 2010; revised March 27, 2011 and May 9, 2011; accepted June 1, 2011. Date of publication July 18, 2011; date of current version February 3, 2012. This work was supported by the South African National Energy Research Institute. Opinions expressed and conclusions arrived at, are those of the author and are not necessarily to be attributed to SANERI.

The authors are with the Department of Electrical and Electronic Engineering, Stellenbosch University, Stellenbosch 7602, South Africa (e-mail: rvermaak@ieee.org; kamper@sun.ac.za).

Digital Object Identifier 10.1109/TIE.2011.2162215

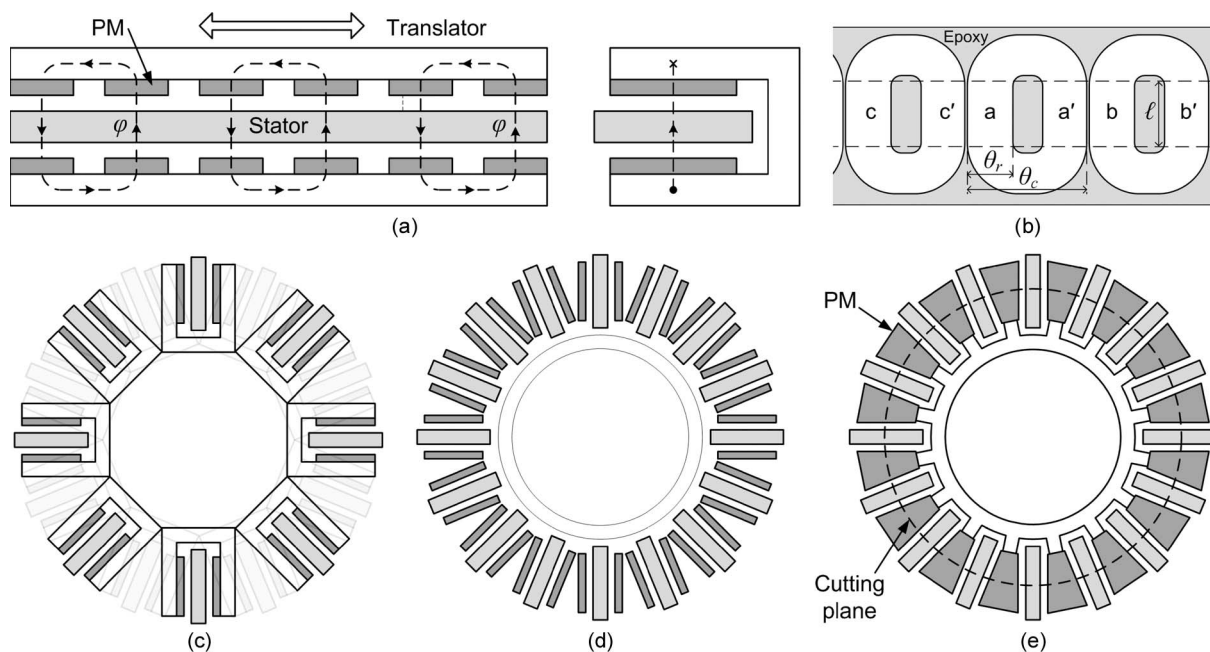


Fig. 1. (a) LDS PM air-cored machine showing pair-wise flux coupling due to the longitudinal ends. (b) Nonoverlapping double layer concentrated air-cored stator windings. (c) A number of LDS machines arranged in a tubular topology, (d) with the yokes removed and (e) with all the adjacent magnets replaced with a single tapered magnet to arrive at the novel topology.

Most WECs work by converting the wave energy captured by the device to a form suitable for driving a standard electrical generator. For instance, oscillating water columns [2], [5] use the heave motion of the waves to create a bidirectional airflow in a chamber; this is then used to drive a standard generator through an air turbine and a gearbox. Each energy conversion stage will require maintenance and incurs losses. For this reason, direct drive WECs using permanent magnet (PM) linear generators have received much attention in recent years [6]–[17]. These WECs use the heave motion of the waves to directly drive a linear generator. Due to the elimination of any mechanical interface between the device and the electrical generator, maintenance and losses are kept to a minimum. In other areas where linear motion is converted to electricity, or vice versa, linear machines are also starting to receive increasing attention for the same reasons, e.g., industrial automation [18], transportation [19], compressor systems [20], and even low power energy storage [21] and solar power [22]. Furthermore, direct drive WECs also contain no hydraulic fluid, like many other WECs [2], which would need replacement (maintenance) or cause concern for the environment if leakage should occur.

However, due to the slow speed of the waves, very large forces need to be reacted by these machines; this means that the devices are physically very large and hence their mass and cost per unit power are also high. The larger the machines, the more difficult it also becomes for bearings to carry the load of the normal attraction forces in iron-cored machines, which means even more structural mass is needed.

The Archimedes wave swing (AWS) was the first device of this kind, developed in the Netherlands and first tested in the sea off the coast of Portugal in 2004 [7]. Different types of conventional linear machines are compared for the AWS in [8]; of these, the longitudinal flux (LF) PM synchronous machine

is found to be the most efficient and to also have the lowest active material cost. The other known linear generators which have made it to sea trials (one from Uppsala University [9] and one from Oregon State University [10]) are also LFPM generators. These generators suffer particularly from high bearing loads and/or cogging forces. Pair-wise flux coupling due to the longitudinal ends of these generators also cause uneven air-gap flux density which, for instance, could render methods for decreasing cogging forces completely ineffective [11].

Some suggestions from Polinder *et al.* [12] for overcoming problems associated with direct drive WECs include: increasing generator speed, investigating higher force density generator types, investigating air-cored machines, and using cheaper construction methods, like using concentrated coil windings.

In [8] and [13], variable reluctance PM machines like transverse flux and vernier hybrid machines are investigated as a high force density alternative to LFPM machines. Unfortunately, difficult construction [8] and low power factor [13] are considerable disadvantages of these machines. Different linear tubular topologies are also reported in [14] and [15], also as higher force density alternatives to planar LFPM machines. High normal attraction forces are, however, still a problem in all of these machines.

One way to completely eliminate attraction forces between the stator and translator, and hence large amounts of structural mass, is to use an air-cored stator. A single-sided linear tubular air-cored generator is investigated in [16], and a similar generator is also used in the WEC manufactured by Trident Energy [17]. The air gap flux density unfortunately decreases dramatically away from the PM translator due to the lack of iron in the stator; this can be compensated for by using a double-sided PM translator as seen Fig. 1(a) [23]–[25]. The so-called C-Gen machine, which is developed at Edinburgh University

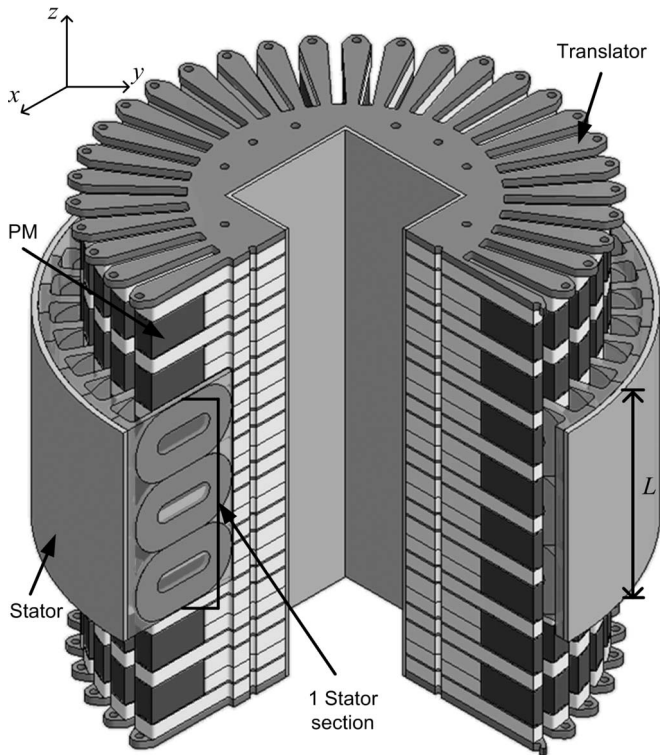


Fig. 2. Three-dimensional cut-out view of the novel linear generator.

[26], is the only generator of this kind currently investigated for use in WECs. With the double-sided translator, normal attraction forces are, however, now present between the two opposing sides of the translator. The pair-wise flux coupling associated with LFPM machines is also still present in linear double-sided (LDS) machines, as seen in Fig. 1(a).

In this paper, the design aspects of a novel air-cored PM machine topology is considered. The novel topology is developed from the LDS topology with the aim to further reduce structural mass and to also eliminate the pair-wise flux coupling associated with LFPM machines. In the next section, the development of the topology is discussed where after the modeling and design optimization are considered. The optimized design is verified with finite element analysis (FEA), and first test results of a prototype generator are presented.

II. LINEAR GENERATOR CONCEPT

As mentioned, the novel generator is developed from the LDS air-cored topology as shown in Fig. 1(a) and (b). A number of these machines can be arranged in a tubular topology as shown in Fig. 1(c). The yokes can then be removed as shown in Fig. 1(d), and the adjacent magnets can be replaced with one trapezoidal magnet as shown in Fig. 1(e); a 3-D cut-out view of the topology can be seen in Fig. 2. A new transverse circulating flux path has now been created; i.e., the flux circulates around the machine, and there is ideally no flux coupling between neighboring poles as in the original machine. This means that the pair-wise flux coupling and its negative effects present in LFPM machines are eliminated. By removing the yoke,

a source of losses and structural mass is also removed. The attraction forces between any two opposing magnets is also ideally zero as each magnet experiences basically equal forces from both sides; this means less structural mass is needed for the magnet support.

The stator windings can consist of normal overlapping or nonoverlapping (NO) windings. NO windings (in literature also referred to as concentrated windings, fractional-slot windings, and some other names [27], [28]) are particularly attractive because of their ease of manufacture and small end windings [25], [29], [30]. The coils can be machine wound and individually inserted into the stator. The smaller end windings mean that less copper is used, which reduce costs and copper losses in the machine. In [25], it is shown that up to 50% less copper is used for a NO air-cored winding compared to a normal overlapping winding. Smaller, flat end windings also mean that the end windings occupy less space.

Studies in [29], [30] show that good winding factors can be obtained for NO windings in high pole number radial flux machines. It has also been shown that the winding factor alone does not determine the performance of NO air-cored windings, but that the coil-side to coil-span ratio κ also plays an important role [25]; it is shown that a pole/coil combination of $4/3$ with $\kappa = 0.37$, although resulting in a fundamental winding factor of only $k_{w1} = 0.875$, also gives the optimal thrust per given copper losses, which is equivalent to efficiency, for double-layer (DL) NO air-cored windings.

Considering the topology of the novel machine, it is clear that at the inside diameter, it is essential to have an end-winding overhang as small as possible in order to fit the maximum number of stator sections into the machine. It is therefore decided to use a NO winding. For NO windings, DL windings also have smaller end windings compared to single-layer windings; a DLNO winding, as shown in Fig. 1(b) is therefore selected.

An analytical model for the novel generator is developed in the next section. This expands on the work presented on the novel topology in [31] and [32].

III. MATHEMATICAL MODELING

A radial cutting plane at the average magnet thickness h_m is introduced to the machine shown in Fig. 1(e). The radial plane is then rolled open into a flat 2-D model as shown in Fig. 3(a). This is similar to how a 2-D model for an axial flux rotary machine is developed [33]. This model basically represents a LDS machine, and as such much of the analytical equations can be derived from literature. These equations are presented in this section and form the basis of the design optimization procedure developed in the next section. The dimensions of the machine can be seen in Fig. 3(a) and (b). The structural and thermal modeling of the machine is beyond the scope of this paper.

As is the principle in all PM synchronous generators, the changing flux observed by the stator due to the translator's relative motion induces an electromotive force (EMF) in the stator coils according to Faraday's law of electromagnetic induction. The air gap flux will therefore first be considered.

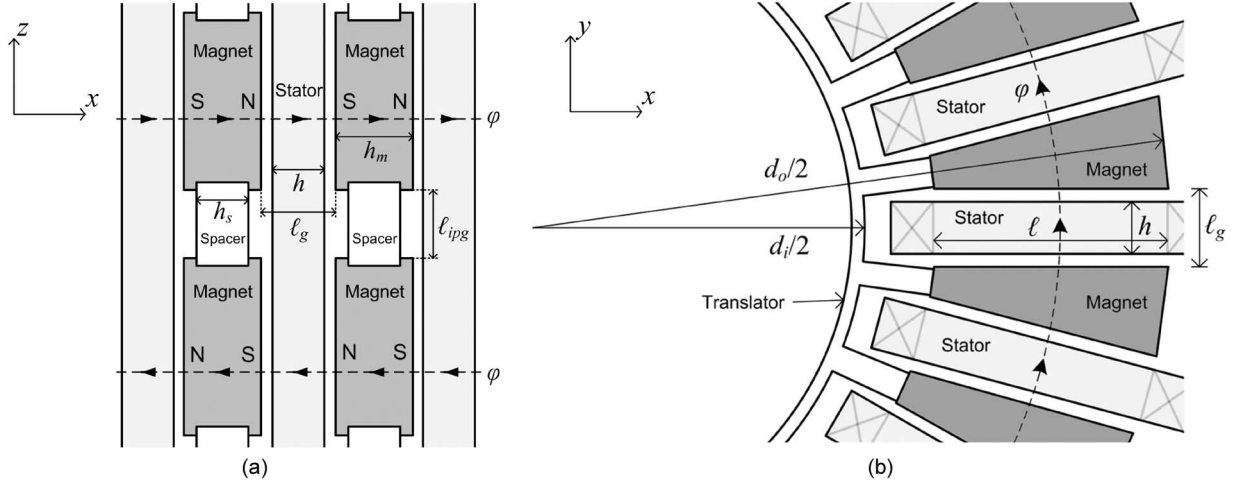


Fig. 3. Dimensions of the novel linear generator as seen (a) from the side and rolled open at the cutting plane of Fig. 1(e) and (b) as seen from the top.

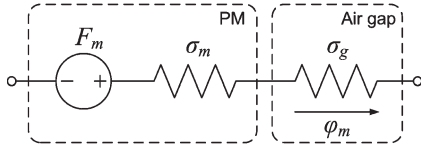


Fig. 4. Magnetic circuit model of one magnet and one air gap.

A. Magnetic Circuit Model

The magneto motive force generated by a single PM is given as

$$F_m = H_c h_m. \quad (1)$$

The reluctance of the air gap and the PM is, respectively, given as

$$\sigma_g = \frac{\ell_g}{\mu_0 A_g} \text{ and } \sigma_m = \frac{h_m}{\mu_{rec} A_m}. \quad (2)$$

The lumped parameter model shown in Fig. 4 represents one PM and one air gap. To represent the complete circuit through which the magnetic flux flows, n_s of the circuits in Fig. 4 must be placed in series. Assuming no leakage flux and applying Kirchoff's voltage law then gives

$$n_s H_c h_m = n_s \varphi_m \left(\frac{h_m}{\mu_{rec} A_m} + \frac{\ell_g}{\mu_0 A_g} \right). \quad (3)$$

Substituting $\mu_{rec} = B_r / H_c$ from the magnet B-H curve into (3) and simplifying give

$$H_c h_m = B_m \left(\frac{H_c}{B_r} \right) h_m + B_p \left(\frac{1}{\mu_0} \right) \ell_g. \quad (4)$$

In the air gap region at the middle of the magnet pole, where the peak flux density B_p is observed, there is no fringing or flux leakage to the adjacent magnet poles, so that it is assumed that the magnet flux density $B_m = B_p$; substituting this into (4) and rearranging then give

$$B_p = \frac{\mu_0 h_m B_r H_c}{\mu_0 h_m H_c + \ell_g B_r}. \quad (5)$$

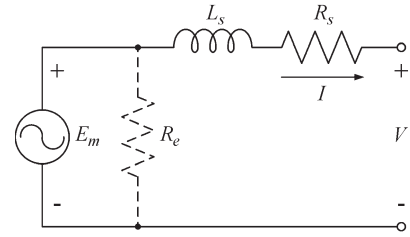


Fig. 5. Per phase equivalent steady state circuit model of the novel machine.

The air gap flux along the length of the translator can now be assumed sinusoidal as

$$B_g = B_{p1} \sin \left(\frac{p\pi}{L} z \right) \quad (6)$$

where the peak fundamental flux density B_{p1} can be calculated from B_p as $B_{p1} = B_p / k_b$. A typical value of $k_b = 0.97$ is obtained from the Fourier transform of FEA-obtained flux density waveforms of previous designs of the novel machine. The more traditional method of using a trapezoidal approximation for the air gap flux density and calculating the fundamental component from this, as used in [34], could also have been used.

B. Stator Equivalent Circuit Model

The steady-state per phase equivalent circuit representing the air-cored stator winding is shown in Fig. 5 [33]. The induced EMF is assumed sinusoidal as

$$e_m(t) = E_p \cos(\omega t) \quad (7)$$

where the peak EMF for NO air-cored windings is derived in [25] as

$$E_p = \frac{2\omega q B_{p1} \ell L N k_{w1}}{\pi p a}. \quad (8)$$

The fundamental winding factor k_{w1} for NO windings is also derived in [25].

Copper losses and eddy-current losses in the copper windings constitute the only sources of losses in the air-cored stator. The

copper losses are represented by the phase resistance in series with the EMF; it is calculated as [25]

$$R_s = \frac{N^2 q \rho_{cu} (2\ell + \ell_e)}{a^2 k_f h w} \quad (9)$$

where the end-winding length is given as

$$\ell_e = \frac{2\theta_c L}{\pi p} (1 - 0.586\kappa). \quad (10)$$

The eddy-current losses can be expressed as [34], [35]

$$P_e = 1.7 N Q n_c \frac{2\pi \ell d_w^4 B_p^2 \omega^2}{32 \rho_{cu}} \quad (11)$$

and is normally represented by a resistor in parallel with the EMF [33]; the eddy losses can however be designed to be very small and will here be considered separately from the circuit model as explained later.

An accurate analytical expression for the inductance of air-cored windings is difficult to find; the specific layout of the stator coils in this machine also further complicates this. However, the synchronous inductance of air-cored machines is generally much smaller than in iron-cored machines, and since this machine will be operating at low frequencies, the synchronous reactance given by $X_s = \omega L_s$ is expected to be negligible. This is further investigated with FEA in Section V-E.

Ignoring the eddy-current losses in Fig. 5, the total instantaneous power generated by the linear generator is given as

$$p_{dt}(t) = 3e_m(t)i(t) = f_{dt}(t)v(t). \quad (12)$$

Assuming that the translator motion is sinusoidal, it can be shown [36] that $p_{dt}(t)$ also varies sinusoidally with an average value of

$$P_{dt} = \frac{3E_p I_p}{4} = \frac{F_p V_p}{2} \quad (13)$$

where the subscript p denotes peak values of the EMF, current, force, and velocity. For simplicity, it is assumed in (13) that the EMF and current are in phase, and also that the force and velocity are in phase.

IV. OPTIMIZATION PROCEDURE

DLNO windings for a LDS PM machine are analyzed in detail in [25]. As discussed in Section II, a pole/coil combination of 4/3 with $\kappa = 0.37$ results in the optimal force per copper losses, independent of the machine dimensions. These values are therefore used in the design. In the proposed design optimization, the mathematical model as presented in the previous section is further developed such that optimal dimensions for minimizing costs associated with the active material in the machine can be obtained, subject to certain performance specification. It is shown that all the machine dimensions can be calculated once values for only four variables are selected.

A. Performance Specification

It has already been mentioned that the linear generator operates at a constantly varying velocity. In order to design for a certain average power, a constant velocity and force, calculated from (13) as $v_s = V_p/\sqrt{2}$ and $F_{dt} = F_p/\sqrt{2}$, respectively, are assumed. The linear generator specifications are now given in terms of the required average power P_{dt} , average velocity v_s , and efficiency η .

The dimensional parameters to be optimized are the generator active length L , winding active length ℓ , stator height h , average magnet height h_m , and the inside and outside diameter d_i and d_o . These dimensions can be seen in Figs. 2 and 3. The dimensional parameters depend on the choice of the number of stator sections n_s , the rms current density J , and the number of active poles p ; these additional parameters therefore also form part of the optimization.

The performance parameters, dimensional parameters, and the additional parameters to be optimized are now, respectively, defined in matrix format by \mathbf{U} , \mathbf{X}_1 , and \mathbf{X}_2 as

$$\mathbf{U} = \begin{bmatrix} P_{dt} \\ v_s \\ \eta \end{bmatrix}; \quad \mathbf{X}_1 = \begin{bmatrix} L \\ \ell \\ h \\ h_m \\ d_i \\ d_o \end{bmatrix}; \quad \mathbf{X}_2 = \begin{bmatrix} n_s \\ J \\ p \end{bmatrix}. \quad (14)$$

By recognizing that each of the stator sections as defined in Fig. 2 are identical, the power P_d generated in one stator section can be calculated as $P_d = P_{dt}/n_s$. Furthermore, two more required performance parameters, which are here also defined for only one stator section, are the developed thrust F_d and the copper losses P_{cu} . The performance specification can now be simplified as

$$\mathbf{G} = \begin{bmatrix} F_d(\mathbf{X}_1, \mathbf{X}_2) \\ P_{cu}(\mathbf{X}_1, \mathbf{X}_2) \end{bmatrix} = \frac{1}{n_s} \begin{bmatrix} 1/v_s \\ k(1-\eta) \end{bmatrix} P_{dt} \quad (15)$$

where $k < 1$ is the ratio of the copper losses to the total losses in the machine. As explained before, only copper losses and the eddy-current losses in the stator windings need to be considered and hence k is given as

$$k = \frac{P_{cu}}{P_{cu} + P_e}. \quad (16)$$

It can be seen from (11) that the determining factor for P_e is the wire diameter d_w . The electrical frequency ω , which also has an effect on P_e , depends on the wave speed and the magnet pole pitch. Due to constraints on the magnet pole pitch (discussed later) and the inherent slow wave speed, ω is expected to be very low. Therefore, by adjusting the number of parallel strands in each coil turn, and so adjusting d_w , P_e can be designed to be very small. Assuming a value of k then serves to reduce the complexity of the problem.

B. Thrust Calculation

Similarly, as derived in [25], the thrust developed per stator section can be expressed as

$$F_d = k_w C_1 K_1 \quad (17)$$

The machine constant C_1 is given by

$$C_1 = B_{p1} \sqrt{\frac{2\kappa k_f P_{cu}}{\rho_{cu}}}. \quad (18)$$

The variable K_1 , which is a function of \mathbf{X}_1 only, is given by

$$K_1 = \sqrt{\frac{h\ell L}{(2 + \delta)}} \quad (19)$$

where δ is the end turn to active stator winding length given as

$$\delta = \ell_e / \ell. \quad (20)$$

It can be noted that K_1 can now be calculated from the required force of (15) and from (17) and (18) as

$$K_1 = \frac{F_d}{k_w C_1}. \quad (21)$$

C. Copper Loss Calculation

The copper losses can be expressed as

$$P_{cu} = K_2 C_2 \quad (22)$$

where C_2 is another machine constant given by

$$C_2 = \kappa k_f \rho_{cu} J^2. \quad (23)$$

The machine constant K_2 , which is also a function of \mathbf{X}_1 only, is given by

$$K_2 = h\ell L(2 + \delta). \quad (24)$$

Similar to (21), K_2 can now be calculated from the required copper losses of (15) and from (22) and (23) as

$$K_2 = \frac{P_{cu}}{C_2}. \quad (25)$$

D. Dimensional Parameter Calculation

The equations from the previous two sections can be manipulated as in [32] to find the active stator winding length ℓ as

$$\ell = \frac{2\theta_c L}{\pi p(K_3 - 2)}(1 - 0.586\kappa) \quad (26)$$

where K_3 is defined as

$$K_3 = \frac{\sqrt{K_2}}{K_1}. \quad (27)$$

According to (26), and since the optimal values for θ_c and κ are known (see [25]), there exists a unique value of ℓ for a given combination of L , p , J , and n_s . Hence, if L , p , J , and n_s are chosen, ℓ can be determined from (26). Furthermore, with ℓ known, h can be determined from (19) or (24).

By rearranging (5), the average magnet height can be calculated as

$$h_m = \frac{B_p \ell_g}{\mu_0 H_c (1 - B_p / B_r)}. \quad (28)$$

The required value of B_p is selected in the design.

An approximation of the outside and inside diameter of the machine is given by

$$d_o = \frac{n_s}{\pi}(\ell_g + h_m) + \ell \quad (29)$$

$$d_i = d_o - 2 \left[\ell + \left(\frac{4\kappa L}{3p} \right) \right] - g. \quad (30)$$

With the values of ℓ , h , and h_m already calculated from (26), (24) and (28), d_o and d_i can now easily be found from (29) and (30).

E. Active Mass Calculation

The active mass consists of the PMs and the stator copper. The PM mass is given by

$$M_m = \gamma_{fe} \tau_m h_m \ell L. \quad (31)$$

A typical value for the per unit magnet width τ_m that can be used in the design is $\tau_m = 0.7$ [33], [34].

The copper mass is given by

$$\begin{aligned} M_{cu} &= \gamma_{cu} \kappa k_f h \ell L (2 + \delta) \\ &= \gamma_{cu} \kappa k_f K_2 \end{aligned} \quad (32)$$

Substituting (23) and (25) into (32) gives the equation for copper mass as

$$M_{cu} = \frac{P_{cu} \gamma_{cu}}{\rho_{cu} J^2}. \quad (33)$$

It can be noted that the copper mass is independent of \mathbf{X}_1 and only a function of n_s and J of \mathbf{X}_2 .

With all the parameters of \mathbf{X}_1 and \mathbf{X}_2 known, the active mass of the generator can be calculated from (31) and (33).

F. Dimensional Constraints

To ensure minimum leakage flux between adjacent magnet poles, the design of the machine is subjected to the following constraints, similarly as given in [34]:

$$\begin{aligned} h_m &> \ell_g \\ \ell_{ipg} &= \frac{L}{p}(1 - \tau_m) > \ell_g \end{aligned} \quad (34)$$

where ℓ_{ipg} is the interpolar gap as defined in Fig. 3(a).

For construction purposes, it is also important to ensure that the minimum magnet height is greater than spacer height h_s as

$$h_{mi} = \frac{\pi}{n_s}(d_o - 2\ell) - \ell_g > h_s. \quad (35)$$

G. Optimization Procedure

The objective function $F(\mathbf{X}_1, \mathbf{X}_2)$ that has to be minimized in the design optimization, subject to the performance constraints of (14) and the dimensional constraints of (34) and (35), can now be expressed as

$$F(\mathbf{X}_1, \mathbf{X}_2) = w_1 M_m(\mathbf{X}_1, \mathbf{X}_2) + w_2 M_{cu}(\mathbf{X}_2) \quad (36)$$

where w_1 and w_2 are weighting factors. By assigning the price per kg of the PM material and copper to w_1 and w_2 , respectively, the objective function represents the active material cost of the machine. This approach of minimizing the active material cost is followed for linear machines in [8] and [16]. It may, however, also be necessary to factor in the labor costs associated with the copper and magnet mass, such as winding the copper onto the stator and fixation of the magnets. Stator winding could be considerably more expensive than magnet fixation, depending on the specific type of machine. To factor in these costs will require foreknowledge of manufacturing procedures and times; this information is hardly ever available at the development stage, but should be considered where possible.

It is clear from (14)–(36) that all the dimensional parameters of \mathbf{X}_1 and the objective function can be determined for a given value of \mathbf{X}_2 and L . This relatively straightforward analytical model allows for optimal dimensions to be obtained by way of an exhaustive optimization procedure. Such a procedure iterates through all the possible combinations of the input variables (\mathbf{X}_2 and L) to find the minimum value of the cost function. A program to do this was implemented in the Python programming language. For each combination of the input variables, the constraints of (34) and (35) are checked; the objective function is only calculated if the constraints are not violated. Through each valid iteration, the values of \mathbf{X}_1 and \mathbf{X}_2 are stored if $F(\mathbf{X}_1, \mathbf{X}_2)$ is less than in the previous iteration. The optimal dimensions are therefore simply retrieved from memory when the program terminates. The flow diagram of the program is shown in Fig. 6.

It is worth pointing out that this procedure is different to other optimization procedures in that each iteration finds the machine dimensions which exactly satisfy the performance specifications of (14). If any of the solutions do not satisfy the constraints of (34) and (35), it is simply discarded. The procedure then basically finds the solution with the minimum value of $F(\mathbf{X}_1, \mathbf{X}_2)$ from the valid solutions. There are therefore no problems with distinguishing between local and absolute maxima like in other optimization algorithms.

The procedure was used for a 2 kW design of the novel topology in [32] and was shown to produce significant reductions in active material over a nonoptimized machine. This, in turn, follows after the nonoptimized machine was shown to compare very favorably with existing experimental iron-cored machines in [31].

V. PROTOTYPE DESIGN

A. Specification and Constant Parameters

It is decided to design a 1 kW machine with an efficiency of 85%. The average translator velocity is chosen as 0.75 m/s, similar to the typical wave conditions in [10]. This gives

$$\mathbf{U} = \begin{bmatrix} P_{dt} \\ v \\ \eta \end{bmatrix} = \begin{bmatrix} 1000 \text{ W} \\ 0.75 \text{ m/s} \\ 85\% \end{bmatrix}. \tag{37}$$

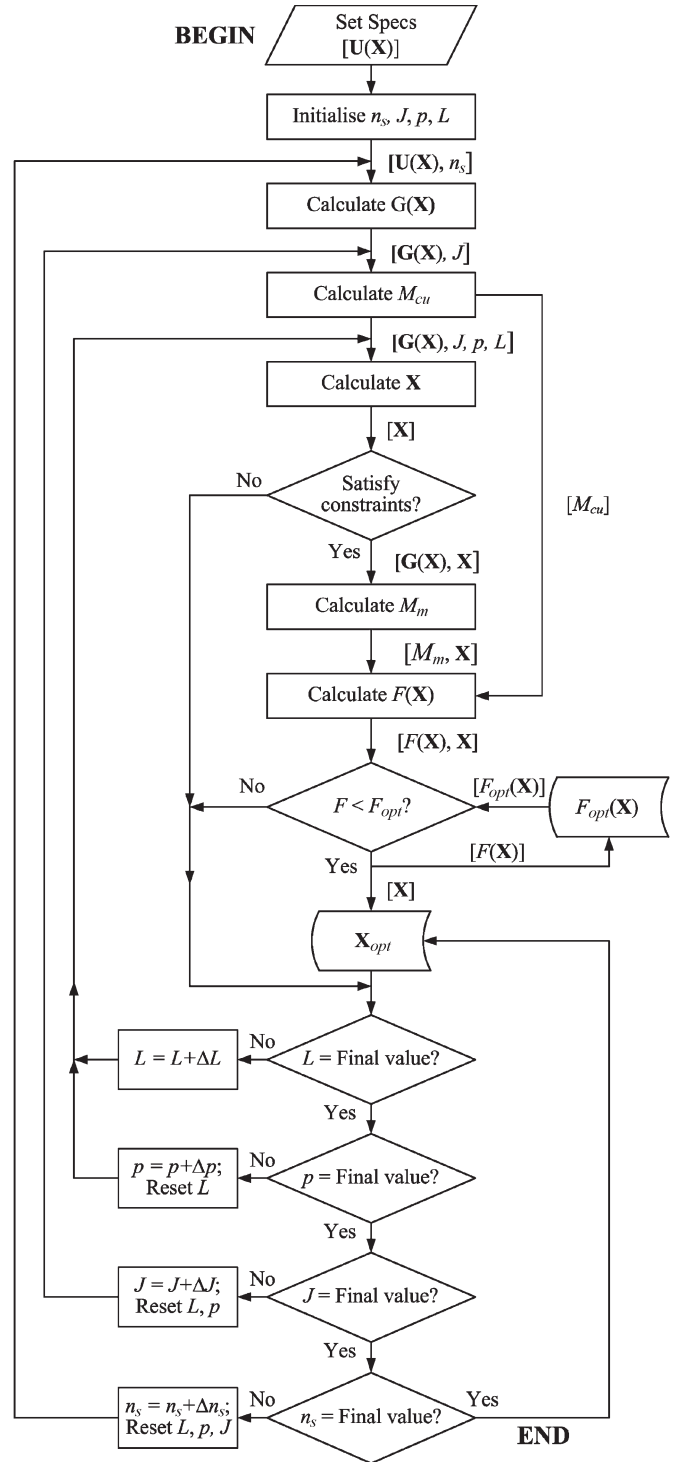


Fig. 6. Optimization procedure flow diagram.

The value of \mathbf{G} of (15) depends on n_s , which is a variable in the optimization; \mathbf{G} will thus be calculated for a range of different values of n_s .

From experience, k of (16) is taken as $k = 0.95$. For the windings, $\kappa = 0.37$ and $\theta_c = 4\pi/3$ are selected according to [25], and $k_f = 0.45$ is also selected from experience.

For the PMs, NdFeB magnets of grade N48 are chosen. A study in [34] shows that by using the highest magnet grade, a reduction in magnet mass can be achieved with only a marginal

TABLE I
 CONSTANT PARAMETERS

ρ_{cu} (Ωm)	1.7×10^8	B_r (T)	1.37
γ_{fe} (kg/m^3)	7580	H_c (kA/m)	1021
γ_{cu} (kg/m^3)	8230	B_p (T)	0.7
κ	0.37	g (mm)	2
k_f	0.45	τ_m (mm)	0.7
k_{w1}	0.875	h_s (mm)	10

 TABLE II
 OPTIMAL DIMENSIONS

Weighting	$w_1 = w_2$	d_o (mm)	466
M_m (kg)	50.73	d_i (mm)	262
M_{cu} (kg)	32.81	ℓ (mm)	65
n_s	38	h (mm)	11.5
J (A/mm^2)	1.45	h_m (mm)	17.5
p	4	h_{mo} (mm)	23
L (mm)	224	h_{mi} (mm)	12

increase in cost. Some of the other constant parameters used in the design are given in Table I.

B. Optimization

The optimization procedure discussed in Section IV-G is used to find the optimal dimensions of the machine, subject to the performance specifications of (37). It is mentioned that both material and labor costs should be considered when deciding on the weighting factors w_1 and w_2 of (36). For the novel topology, copper wire is sourced locally and the magnets from abroad. The magnet price is 4.5 times the copper price. However, the PMs could simply be slid into place in the machine; this is a fast and easy process. The stator coils each had to be stranded and wound around a former. After this, the coils had to be potted in epoxy resin and then bolted to the stator ring. It is as such anticipated that the labor costs associated with the copper far exceed the labor costs associated with the magnets. It is decided to use $w_1 = w_2$ in the optimization. The results of the optimization are given in Table II.

In Fig. 7, the magnet mass for different valid solutions calculated in the optimization procedure, i.e., solutions satisfying the constraints of (34) and (35), are shown. It is interesting to note that for the optimal combination of $p = 4$ and $J = 1.45 \text{ A}/\text{mm}^2$, only one valid solution exist. As J is decreased and/or p is increased, more valid solutions exist. The maximum allowable valid value of J therefore gives both the minimum M_m and M_{cu} [from (33)] and therefore also the minimum value of the objective function. What is even more interesting is that, due to this, when the optimization is repeated with $w_1 = 4.5w_2$ to reflect only the active material price in the optimization, the

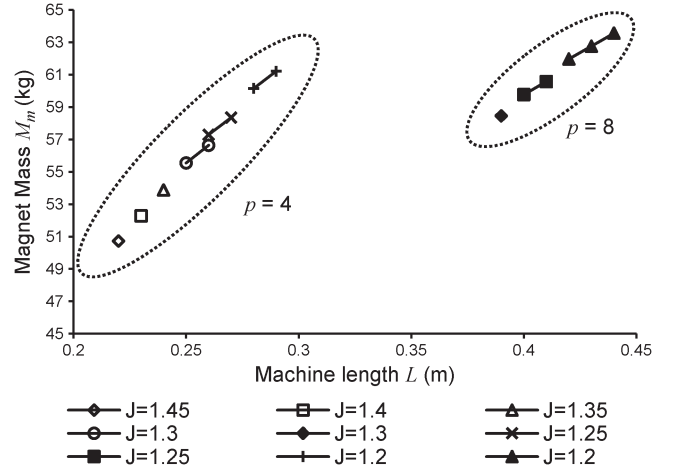


Fig. 7. PM mass as a function of active machine length L , number of poles p , and current density J . Only valid solutions are shown.

same optimum dimensions is returned as before. The optimum dimensions can therefore be obtained by minimizing only the magnet or only the copper mass (or cost).

C. Winding Design

The required output voltage is determined by the intended load. Plans for this generator include testing with an active IGBT rectifier with a dc-bus voltage of 300 V. It is as such decided to limit the output phase voltage to below 150 V. By ignoring the internal voltage drop and limiting the peak EMF of (8) at the peak velocity to below 150 V, an added degree of safety exists. With all the coils of each phase in series and $N = 40$, $E_p = 128 \text{ V}$ at the maximum velocity of $V_p = 1.06 \text{ m/s}$.

The number of parallel strands per turn must be selected in order to have a wire diameter sufficiently small to limit the eddy-current losses as explained in Section IV-A. Selecting $n_c = 16$ results in $d_w = 0.52 \text{ mm}$ and $P_e = 0.007 \text{ p.u.}$, which corresponds well with the chosen value of $k = 0.95$ [from (16)]. The stator thickness h was reduced from 11.5 to 11 mm for the experimental machine; this was done simply to create a slightly larger mechanical air gap g to help provide some leniency on the manufacturing tolerances. This inevitably means a small loss in performance will be experienced. The parameters calculated based on the design choices explained here are given in Table III; it reflects the loss of average power to 953 W.

D. Translator Length and Drive System

The wave height of the intended installation site for a WEC would determine the stroke length of the linear generator. Assuming that the stator winding should at all times be within the PM generated field, the translator length must then equal the stator length plus the stroke length. Space and financial constraints meant that it was not possible to construct a translator and a drive system long enough to simulate a realistic wave height (which is in the order of meters).

It is also decided to investigate the effect of the translator moving completely out of the stator at the stroke ends while at the same time saving on the magnet costs. A low speed, high

TABLE III
ANALYTICAL AND FEA-OBTAINED PARAMETERS

$v = 0.75$ m/s	Analytical	FEA
B_p (T)	0.7	0.69
E_p (V)	90.7	95.7
R_s (Ω)	1.9	1.9
L_s (mH)	-	6
F_{dt} (N)	1271	1342
P_{dt} (W)	953	1007
P_{cu} (p.u.)	0.146	0.146
P_e (p.u.)	0.007	-
η (%)	84.7	-

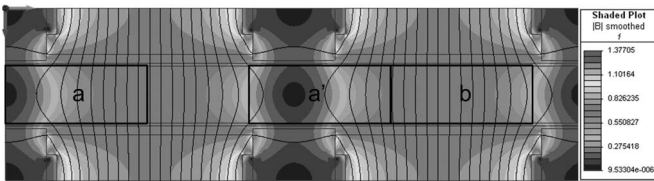


Fig. 8. FE models showing flux lines and flux density color plot.

pole number PM motor with a crank is used to drive the linear generator. The drive motor’s diameter of about 0.7 m means that a stroke length of the same dimension could be achieved. With the pole width already determined, an eight-pole translator was chosen for the translator to move out of the stator ends with the given stroke length.

E. Finite Element Analysis

FEA is used to verify the analytical design. The 2-D model developed in Section III is implemented in the FE package Infolytica Magnet 7 with appropriate boundary conditions. In Fig. 8, a color flux density and contour plot are shown of two poles of the model; this serves to illustrate how the flux actually flows in this machine. This includes fringing at the ends of the poles and also a degree of flux leakage between adjacent magnets. The peak air gap flux density is found to be 0.69 T, which is very close to the analytically obtained value of 0.7 T.

Magnetostatic solutions were obtained with the translator at different positions relative to the stator. The three-phase EMFs obtained from the time derivative of the flux linkages at the different positions through 2π electrical radians are shown in Fig. 9; a constant velocity equal to the design velocity is simulated. In Fig. 10, the force on the translator is also shown. This is simulated by forcing current through the coils, in phase with the EMFs. The FE obtained parameters of the machine are given in Table III together with the analytically obtained values. Overall, good agreement exists between the analytical and FE values. The FE-obtained EMF is slightly higher than the analytical value, which is why the FE-obtained force is also higher than the analytical value by the same percentage. It is

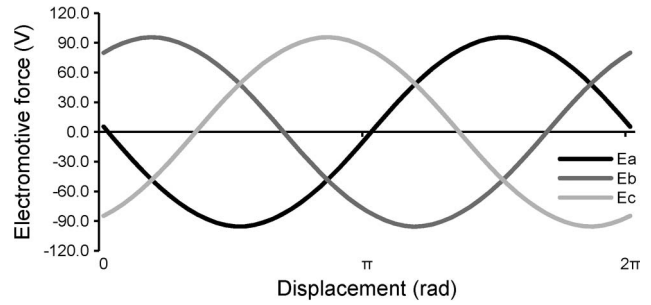


Fig. 9. Simulated generator EMFs with $v = 0.75$ m/s.

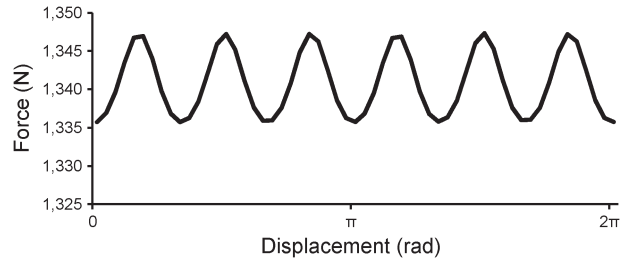


Fig. 10. Simulated generator force with $v = 0.75$ m/s.

worth noting the high quality of the voltage waveforms, which exhibit less than 0.1% THD. The force ripple is also less than 1%. The synchronous phase inductance is also determined and is given in Table III.

As mentioned, the actual machine is designed such that the translator can move completely out of the stator on both ends of its stroke. This case is therefore also simulated with a sinusoidal varying velocity. The EMFs obtained from this is shown in Fig. 12. It can be seen how first the one phase, followed by the other two, becomes active. During the middle of the stroke, the three phases are clearly balanced where after the same effect is repeated as the translator moves out of the stator.

VI. TEST RESULTS

The designed 1 kW linear generator is built and mounted horizontally for laboratory testing and can be seen in Fig. 11. Since the stator is so much lighter than the translator, it was decided to keep the translator stationary while moving the stator. More details of the construction will be presented in future work. It must however be mentioned that the experimental machine demonstrates that very little structural mass is needed to keep the PMs in place. The structural material mostly consists of low density nonmagnetic materials and very little steel. The assumption of a reduction in structural mass is therefore confirmed.

The impedance of the stator is measured by applying a three-phase ac voltage to the windings and measuring the current while the stator is outside the PM field. These measurements are also verified with an LCR meter. The measured resistance is 2.1 Ω which is slightly higher than calculated. This can partly be explained by the interconnections between the 38 stator sections which is not considered in the calculated values. The measured inductance is 8 mH which is also slightly higher than the FE obtained values—this can be ascribed to the fact that the

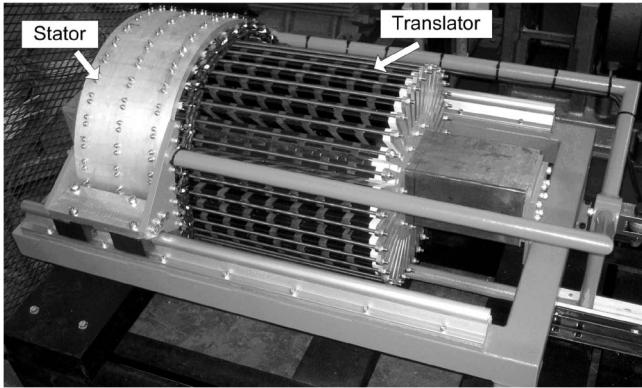


Fig. 11. Novel air-cored PM linear generator as built.

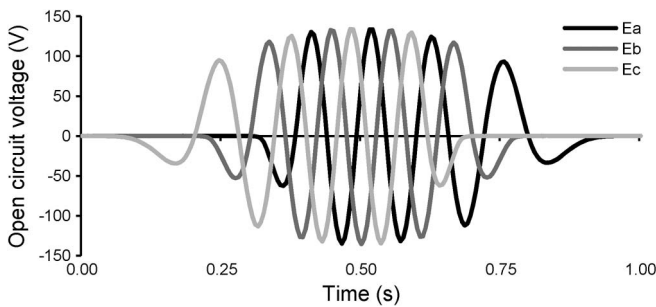


Fig. 12. FEA-simulated generator EMFs during one stroke.

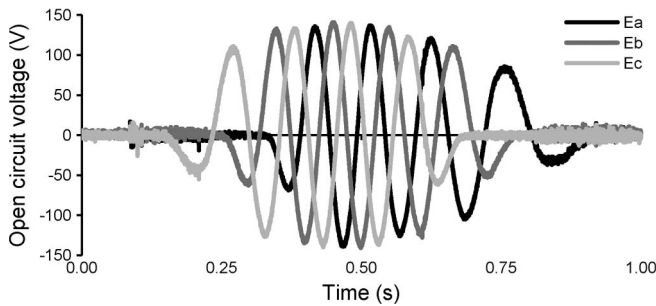


Fig. 13. Measured generator EMFs during one stroke.

2-D FE model does not simulate the effect of the end windings on the inductance. The degree to which the coupling between the different stator sections are simulated correctly is also not sure. 3-D FEA would need to be done to further investigate this aspect.

The measured three-phase open circuit voltage is shown in Fig. 13. Due to nonidealities in the chosen drive system, it was not possible to control the stator velocity to be exactly sinusoidal. However, the envelope of the voltage waveforms compares very well with that of the simulated FE waveforms in Fig. 12. The comparison of the measured and simulated a-phase voltage shown in Fig. 14 also confirms the excellent agreement between the measured and simulated values.

The linear generator is connected to a resistive load and, the terminal voltage and current of the a-phase can be seen in Fig. 15. Again, due to drive system limitations, full load conditions could not be tested, although these first load tests serve to illustrate the correct functioning of the generator as

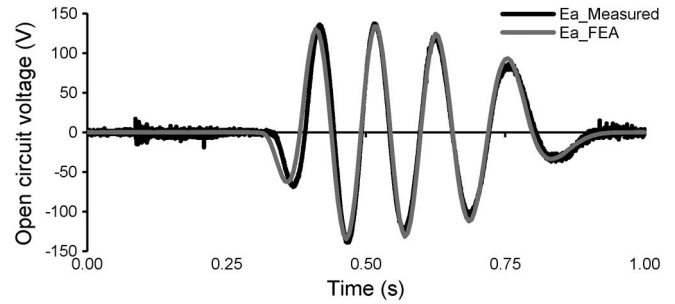


Fig. 14. Comparison of a-phase simulated and measured generator EMFs.

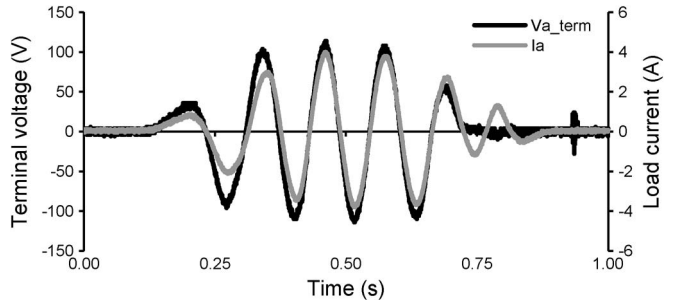


Fig. 15. Measured generator terminal voltage and load current.

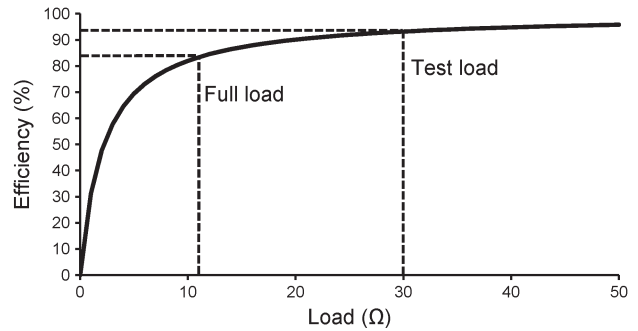


Fig. 16. Calculated generator efficiency for a variation in load.

well as the near unity power factor achieved, even if only at part load.

It is mentioned that the chosen drive system is not ideal. A large amount of mechanical losses are currently present in the system, which, together with the constantly changing velocity and load, makes it impossible to measure the efficiency of the drive system and the generator. However, since the eddy-current losses in the generator are negligible, copper losses constitute the only real source of losses in the machine as mentioned before. It can therefore be shown that the generator efficiency can be approximated as

$$\eta = \frac{R_l}{R_l + R_s} \times 100\% \tag{38}$$

where R_l is the load resistance. Using the measured value of R_s , the efficiency from (38) is shown for a variation in the load in Fig. 16. The efficiency at the test conditions can be seen to be close to 95%, whereas at full load, it is only slightly less than the designed value of 85%.

In the design, only the generator EMF is considered and the terminal voltage largely ignored. It is worth mentioning that the

terminal voltage as a percentage of the EMF can be shown to equal the efficiency as given in (38) and as shown in Fig. 16.

VII. CONCLUSION

The following conclusions can be drawn from the work presented in this paper.

- 1) A novel topology for a linear PM generator, developed from a LDS topology, is presented which eliminates pair-wise flux coupling found in longitudinal flux linear machines. Attraction forces between the stator and translator are eliminated due to the air-cored stator. Attraction forces between the opposing translator sides of LDS machines are also ideally eliminated with the novel topology. The elimination of magnetic attraction forces means a reduction of structural mass can be expected.
- 2) An analytical 2-D model is developed for the novel topology. An exhaustive optimization procedure based on this relatively simple model is also developed and enables optimal dimensions for minimum active mass to be obtained quickly.
- 3) Optimal dimensions for the generator are obtained at the maximum allowable current density and minimum allowable number of poles. At this particular combination of current density and poles, only one solution exists which satisfies the dimensional constraints and gives both the minimum magnet and copper mass. The optimal dimensions can therefore be obtained by minimizing only the magnet or only the copper mass.
- 4) FEA is used to verify the constant velocity analytical design with good results. Output for the practical implementation of the generator at a constantly varying velocity is also produced with FEA.
- 5) The feasibility of implementing the novel topology on a small scale is proven with the construction of a 1 kW prototype generator. Very little structural mass for magnet support is used.
- 6) First test results of the novel generator agree very well with the FE simulated and analytical results and hence confirm the validity of the modeling and design methods as well as the correct functioning of the generator.
- 7) Test results show a near unity power factor for the novel generator which plays an important role in achieving a good efficiency; the efficiency can be approximated from the measured data to be close to 95% at the test conditions.

REFERENCES

- [1] T. W. Thorpe, "A brief review of wave energy: A report produced for the UK Department of Trade and Industry," U.K. Dept. Trade Ind., Westminster, U.K., ETSU-R120, May 1999.
- [2] "2008 Annual report: Implementation agreement of ocean energy systems," Int. Energy Agency, Implementing Agreement Ocean Energy Syst., Paris, France, IEA-OES, 2008.
- [3] J. Falnes, "A review of wave-energy extraction," *Marine Struct.*, vol. 20, no. 4, pp. 185–201, Oct. 2007.
- [4] World Energy Council, T. W. Thorpe, *Wave Energy: 2007 Survey of Energy Resources*, Sep. 2007.
- [5] M. Amundarain, M. Alberdi, A. J. Garrido, and I. Garrido, "Modeling and simulation of wave energy generation plants: Output power control," *IEEE Trans. Ind. Electron.*, vol. 58, no. 1, pp. 105–117, Jan. 2011.
- [6] M. A. Mueller, H. Polinder, and N. Baker, "Current and novel electrical generator technology for wave energy converters," in *Proc. IEEE IEMDC*, Antalya, Turkey, 2007, vol. 2, pp. 1401–1406.
- [7] H. Polinder, M. E. C. Damen, and F. Gardner, "Design, modelling and test results of the AWS PM linear generator," *Eur. Trans. Elect. Power*, vol. 15, no. 3, pp. 245–256, May/Jun. 2005.
- [8] H. Polinder, B. C. Mecrow, A. G. Jack, P. G. Dickinson, and M. A. Mueller, "Conventional and TFPM linear generators for direct-drive wave energy conversion," *IEEE Trans. Energy Convers.*, vol. 20, no. 2, pp. 260–267, Jun. 2005.
- [9] O. Danielsson, M. Eriksson, and M. Leijon, "Study of a longitudinal flux permanent magnet linear generator for wave energy converters," *Int. J. Energy Res.*, vol. 30, no. 14, pp. 1130–1145, Nov. 2006.
- [10] J. Prudell, M. Stoddard, E. Amon, T. K. A. Brekken, and A. von Jouanne, "A permanent-magnet tubular linear generator for ocean wave energy conversion," *IEEE Trans. Ind. Appl.*, vol. 46, no. 6, pp. 2392–2400, Nov./Dec. 2010.
- [11] O. Danielsson and M. Leijon, "Flux distribution in linear permanent magnet synchronous machines including longitudinal end effects," *IEEE Trans. Magn.*, vol. 43, no. 7, pp. 3197–3201, Jul. 2007.
- [12] H. Polinder, M. A. Mueller, M. Scutto, and M. G. de Sousa Prado, "Linear generator systems for wave energy conversion," in *Proc. 7th Eur. Wave Tidal Energy Conf.*, Porto, Portugal, 2007, pp. 1–8.
- [13] M. A. Mueller and N. J. Baker, "Modelling the performance of a vernier hybrid machine," *Proc. Inst. Elect. Eng.—Elect. Power Appl.*, vol. 150, no. 6, pp. 647–654, Nov. 2003.
- [14] V. D. Colli, P. Cancelliere, F. Marignetti, and R. Di Stefano, "A tubular-generator drive for wave energy conversion," *IEEE Trans. Ind. Electron.*, vol. 53, no. 4, pp. 1152–1159, Aug. 2006.
- [15] D. M. Joseph and W. A. Cronje, "Design and analysis of a double-sided tubular linear synchronous generator with particular application to wave-energy conversion," in *Proc. IEEE PES Power Africa*, Johannesburg, South Africa, Jul. 2007, pp. 1–8.
- [16] R. Crozier and M. Mueller, "Modelling and first order optimisation of the air-cored tubular PM machine using polynomial approximation," in *Proc. Int. Conf. Elect. Mach.*, Vilamoura, Portugal, Sep. 2008, pp. 1–6.
- [17] P. C. J. Clifton, R. A. McMahon, and H. P. Kelly, "Design and commissioning of a 30 kW direct drive wave generator," in *Proc. IET 5th Int. Conf. Power Electron., Mach. Drives*, Brighton, U.K., 2010, pp. 1–6.
- [18] C. Bianchini, F. Immovilli, M. Cocconcelli, R. Rubini, and A. Bellini, "Fault detection of linear bearings in brushless ac linear motors by vibration analysis," *IEEE Trans. Ind. Electron.*, vol. 58, no. 5, pp. 1684–1694, May 2011.
- [19] R. Appunn, B. Schmülling, and K. Hameyer, "Electromagnetic guiding of vertical transportation vehicles: Experimental evaluation," *IEEE Trans. Ind. Electron.*, vol. 57, no. 1, pp. 335–343, Jan. 2010.
- [20] J. Wang, D. Howe, and Z. Lin, "Design optimization of short-stroke single-phase tubular permanent-magnet motor for refrigeration applications," *IEEE Trans. Ind. Electron.*, vol. 57, no. 1, pp. 327–334, Jan. 2010.
- [21] J. Wang, W. Wang, G. W. Jewell, and D. Howe, "A low-power, linear, permanent magnet generator/energy storage system," *IEEE Trans. Ind. Electron.*, vol. 49, no. 3, pp. 640–648, Jun. 2002.
- [22] J. Schutte and J. M. Strauss, "Optimisation of a transverse flux linear PM generator using 3D finite element analysis," in *Proc. 19th Int. Conf. Elect. Mach.*, Rome, Italy, Sep. 2010, pp. 1–6.
- [23] G.-H. Kang, J.-P. Hong, and G.-T. Kim, "A novel design of an air-core type permanent magnet linear brushless motor by space harmonics field analysis," *IEEE Trans. Magn.*, vol. 37, no. 5, pp. 3732–3736, Sep. 2001.
- [24] S. Vaez-Zadeh and A. H. Isfahani, "Multi-objective design optimisation of air-core linear permanent-magnet synchronous motors for improved thrust and low magnet consumption," *IEEE Trans. Magn.*, vol. 42, no. 3, pp. 446–452, Mar. 2006.
- [25] M. J. Kamper, "Comparison of linear permanent magnet machine with overlapping and non-overlapping air-cored stator windings," in *Proc. IET 4th Int. Conf. Power Electron., Mach. Drives*, York, U.K., 2008, pp. 767–771.
- [26] N. Hodgins, O. Keysan, A. McDonald, and M. Mueller, "Linear generator for direct drive wave energy applications," in *Proc. Int. Conf. Elect. Mach.*, Rome, Italy, 2010, pp. 1–6.
- [27] A. M. El-Refai, "Fractional-slot concentrated-windings synchronous permanent magnet machines: Opportunities and challenges," *IEEE Trans. Ind. Electron.*, vol. 57, no. 1, pp. 107–121, Jan. 2010.

- [28] J. J. Germishuizen and M. J. Kamper, "Classification of symmetrical non-overlapping three-phase windings," in *Proc. Int. Conf. Elect. Mach.*, Rome, Italy, 2010, pp. 1–6.
- [29] J. Cros and P. Viarouge, "Synthesis of high performance PM motors with concentrated windings," *IEEE Trans. Energy Convers.*, vol. 17, no. 2, pp. 248–253, Jun. 2002.
- [30] F. Magnussen and C. Sadarangani, "Winding factors and joule losses of permanent magnet machines with concentrated windings," in *Proc. IEEE Int. Elect. Mach. Drives Conf.*, Madison, WI, 2003, pp. 333–339.
- [31] R. Vermaak and M. J. Kamper, "Novel permanent magnet linear generator topology for wave energy conversion," in *Proc. IET Int. Conf. Power Electron. Mach. Drives*, Brighthelm, U.K., 2010, p. 6.
- [32] R. Vermaak and M. J. Kamper, "Design of a novel air-cored permanent magnet linear generator for wave energy conversion," in *Proc. Int. Conf. Elect. Mach.*, Rome, Italy, 2010, pp. 1–6.
- [33] R.-J. Wang, M. J. Kamper, K. van der Westhuizen, and J. F. Gieras, "Optimal design of a coreless stator axial flux permanent-magnet generator," *IEEE Trans. Magn.*, vol. 41, no. 1, pp. 55–64, Jan. 2005.
- [34] J. A. Stegmann and M. J. Kamper, "Design aspects of double-sided rotor radial flux air-cored permanent magnet wind generators," *IEEE Trans. Ind. Appl.*, vol. 47, no. 2, pp. 767–778, Mar. 2011.
- [35] R.-J. Wang and M. J. Kamper, "Calculation of eddy current loss in axial field permanent-magnet machine with coreless stator," *IEEE Trans. Energy Convers.*, vol. 19, no. 3, pp. 532–538, Sep. 2004.
- [36] P. R. M. Brooking and M. A. Mueller, "Power conditioning of the output from a linear vernier hybrid permanent magnet linear generator for use in direct drive wave energy converters," *Proc. Inst. Elect. Eng.—Gener. Transm. Distrib.*, vol. 152, no. 5, pp. 673–681, Sep. 2005.



Rieghard Vermaak (M'11) received the B.Eng. degree in electrical and electronic engineering from the University of Stellenbosch, Stellenbosch, South Africa, in 2008, where he is currently working toward the M.Sc.Eng. degree in electrical engineering.

His current research interests are wind and ocean wave power generation and grid integration of renewable energy systems.



Maarten J. Kamper (M'96–SM'08) received the M.Sc. (Eng.) and Ph.D. (Eng.) degrees both from the University of Stellenbosch, Stellenbosch, South Africa, in 1987 and 1996.

He has been with the academic staff of the Department of Electrical and Electronic Engineering, University of Stellenbosch, since 1989, where he is currently a Professor of electrical machines and drives. His research interests include computer-aided design and the control of reluctance, permanent magnet and induction electrical machine drives with

applications in electric transportation and renewable energy. He is a South African National Research Foundation Supported Scientist and a Registered Professional Engineer in South Africa.